Electron localization on dislocations in metals: Real-space first-principles calculations

O. Yu. Kontsevoi,[1] Yu. N. Gornostyrev,[1,2] O. N. Mryasov,[1] A. J. Freeman,[1] M. I. Katsnelson,[2] and A. V. Trefilov[3]
[1]*Department of Physics and Astronomy, Northwestern University, Evanston, Illinois 60208-3112*
[2]*Institute of Metal Physics, Ekaterinburg, Russia*
[3]*Russian Science Center "Kurchatov Institute," Moscow 123182, Russia*
(Received 29 December 2000; revised manuscript received 12 April 2001; published 11 September 2001)

The electronic structure of different types of dislocations in $B2$ intermetallic NiAl and bcc transition metals was investigated using the first-principles real space tight-binding linear-muffin-tin-orbital recursion method. An unusual localization of electronic states inside the valence band is observed in the cores of $\langle 100\rangle\{010\}$ and $\langle 100\rangle\{011\}$ edge dislocations but not in $\langle 111\rangle\{011\}$ edge dislocations. The nature of these localized electronic states and mechanisms for their appearance are analyzed. We show that conditions of electron localization are (i) a decrease of the number of nearest neighbors (''broken bonds'') around the central atom of the dislocation core, (ii) a specific local symmetry of the atomic arrangement in the region of the dislocation core, and (iii) the contribution of d states to the formation of these interatomic bonds. We illustrate our conclusions by demonstrating that electron localization also occurs in $\langle 100\rangle\{010\}$ edge dislocations in bcc metals W, Fe, and Ni. In contrast to semiconductors, the electron localization in metals takes place on bonding orbitals, and will therefore have a significant impact on dislocation energetics and chemical bonding. We suggest that localized electronic states can give a significant contribution to impurity-dislocation interactions in NiAl and other $B2$ intermetallics such as CoTi, CoHf, and CoZr.

DOI: 10.1103/PhysRevB.64.134103 PACS number(s): 61.72.Lk, 71.20.Lp, 71.23.An

I. INTRODUCTION

First-principles calculations of structural, electronic, magnetic, and other physical properties of single crystals have become a traditional and necessary part of materials design. However, only first steps have been taken in understanding the interplay between peculiarities of the electronic structure, defect properties and the mechanical behavior of materials.[1–5] There is numerous pertinent experimental evidence indicating the importance of understanding such an interplay, notably, (i) solid solution hardening effects,[6,7] (ii) changes of mechanical properties during the transition to a superconducting state,[8] (iii) control of the mechanical properties of semiconductors by doping with electrically active impurities,[9] and (iv) magnetoplastic effects.[10] While the mechanisms governing the mechanical response of solids are extremely complex, one of the most important factors is the structure and mobility of dislocations.[11] These defects are always present in real materials and can also have a significant influence on a number of physical characteristics.

At present, theoretical investigations of dislocations are mostly based on classical molecular dynamics (MD) simulations with embedded-atom type interatomic potentials.[12] However, a correct account for changes of the electronic structure due to the introduction of defects into a parent crystal apparently lies beyond the limits of such approaches. These changes may have a significant influence on the structure and the energy of dislocations and, as demonstrated recently,[13] can lead to qualitative changes in the usually assumed picture of dislocation motion in metals.

The role of changes of the electronic structure due to the presence of dislocations has been studied mostly for dislocations in semiconductors.[14] Due to covalent bonding in these materials, ''broken bonds'' appear in the dislocation core, and a ''dislocation level'' arises in the electronic spectrum inside a fundamental gap.[15] This leads to core reconstruction[16] and has a significant influence on the interaction of the dislocation with point defects.[17] Other examples are ionic crystals, where the cores of edge dislocations possess an extra charge. The resulting electrostatic terms turn out to be the main contributor to the Peierls relief energy in ionic materials.[18]

In metals, in contrast to semiconductors, a simple intuitive model description of the electronic states on a dislocation in ''broken bond'' terms may not be acceptable due to the itinerant nature of conduction electrons,[19] that should effectively screen any excess charge density. However, there is numerous experimental evidence showing the importance of electronic factors in the properties of dislocations and their interaction with other defects in metals.[6,7,10] In particular, the so-called ''extra'' solid solution hardening effect in metals,[7] and especially in intermetallics,[6] is connected with electronic structure peculiarities rather than with a size misfit factor (see discussion in Refs. 4,20,21). Systematic theoretical studies of this problem are almost absent in the literature. An attempt[21] to study electronic states on dislocations in the framework of the single band tight-binding (TB) model Hamiltonian demonstrated, for a specific type of dislocation, Burgers vectors, set of TB parameters, and lattice symmetries, that there is a possibility of the appearance of well-defined localized electronic states in the dislocation core.[21] For edge dislocations, for example, the appearance of localized states was found to be most probable for dislocations with $\langle 100\rangle$ Burgers vector. However, it was not clear from these results if the observed picture of electron localization will remain in *ab initio* all-electron calculations for real metals.

NiAl belongs to the group of $B2$ intermetallics where plastic deformation is carried out mostly by dislocations with $\langle 100\rangle$ Burgers vector and $\{001\}$ and $\{011\}$ glide planes,

except for ''hard'' orientations, where $\langle 111 \rangle$ dislocations become carriers.[23] Here we present the results of first-principles electronic structure calculations for high-temperature intermetallic NiAl in the presence of the $\langle 100 \rangle \{010\}$,[22] $\langle 100 \rangle \{011\}$, and $\langle 111 \rangle \{011\}$ edge dislocations. We investigate conditions for the appearance of localized electronic states depending on the type of dislocation, atomic coordination geometry in the core and the character of interatomic bonds, and demonstrate that these conditions are satisfied for edge dislocations with $\langle 100 \rangle$ Burgers vector in *d*-metals with bcc and *B*2 lattices. Based on the results obtained, we reveal the mechanisms for appearance of these electronic states that are unusual for metals. We also analyze the effect of relaxation of the dislocation core on the energetics and electronic structure of the $\langle 100 \rangle \{010\}$ edge dislocation. We discuss the role of lattice distortions in the dislocation core on electronic states near the Fermi energy, their possible contribution to transport properties, and the effect of relaxation on these states. To justify our findings, we also perform electronic structure calculations for $\langle 100 \rangle$ edge dislocations in bcc transition metals (Ni, Fe, W). Finally, we discuss the effect of electron localization and other peculiarities of the electronic structure of dislocations on energetics of impurity-dislocation interactions, and on the mechanical and other macroscopic properties of metals and alloys.

II. METHODOLOGY

For the electronic structure calculations on dislocations, we applied the first-principles real-space tight-binding linear muffin-tin orbital recursion method[24–26] (TB-LMTO-REC), where the Hamiltonian is constructed *ab initio* in real space using the TB-LMTO formalism[27,28] in the atomic sphere approximation (ASA), and the recursion technique[29] is used to solve the one-electron Schrödinger equation. The local density approximation (LDA) with the von Barth-Hedin form[30] of the exchange-correlation potential was used, and the procedure of Beer and Pettifor[31] was exploited for the correct termination of the recursion continued fractions. The atomic sphere radii were chosen according to the charge neutrality condition, and were adjusted automatically during iterations toward self-consistency to satisfy this condition. This approach allows us to considerably simplify the calculations for systems without crystalline symmetry, because in the case of charge neutral atomic spheres the Madelung term in the potential, which accounts for the long-ranged electrostatic interaction between charged atomic spheres, becomes equal to zero.

To verify the accuracy of the method, the precision of the self-consistent scheme employed, and the dependence of the results on the computational parameters, we calculated the total energy-volume dependence and the equilibrium volume for NiAl. The only parameters of the TB-LMTO-REC method are the length of the recursion continued fractions, the size and the shape of the real-space cluster representing the bulk material, and the presence or absence of periodic boundary conditions for the continued fraction propagation. The results are presented in Fig. 1 for clusters of cubic shape. The calculated equilibrium lattice constant of NiAl ($a = 2.824$ Å) is in good agreement with results of conventional band structure methods: TB-LMTO $a = 2.85$ Å (Ref. 32), ASW $a = 2.86$ Å (Ref. 33), full-potential LMTO $a = 2.839$ Å (Ref. 34), FLAPW $a = 2.836$ (Ref. 35), as well as with experiment (2.887 Å). The underestimated theoretical values of the lattice constant (1–2 %) are typical for LDA calculations. As seen from Fig. 1, the equilibrium volume does not change as the parameters of the computation scheme vary.

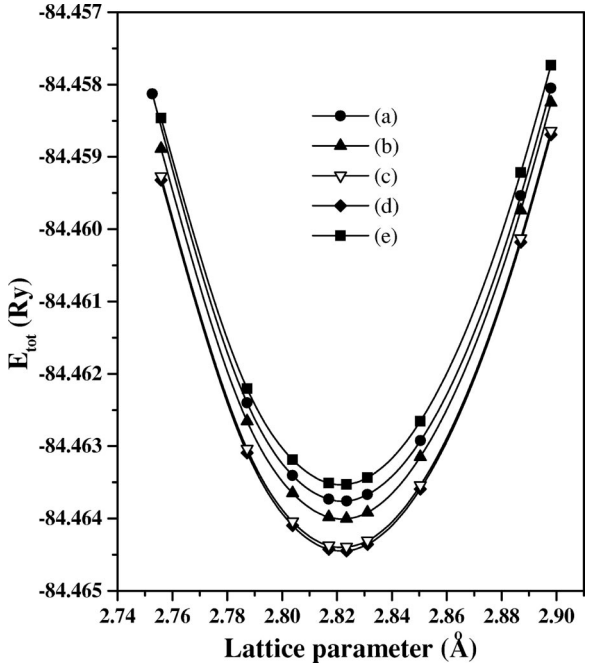

FIG. 1. Total energy as a function of the lattice constant for bulk NiAl, calculated using (a) a cluster of 1000 atoms with free boundary conditions and 30 levels of recursion for *d* electrons, (b) a cluster of 1000 atoms with periodic boundary conditions and 30 levels of recursion, (c) a cluster of 2000 atoms with periodic boundary conditions and 30 levels of recursion, (d) a cluster of 10 000 atoms with periodic boundary conditions and 30 levels of recursion, (e) a cluster of 1000 atoms with periodic boundary conditions and 50 levels of recursion.

The optimal length of the recursion continued fractions is found to be 10 for *s* electrons, 20 for *p* electrons, and 30 for *d* electrons. A further increase in the number of recursion levels actually decreases the accuracy, as seen from a comparison of the total energy curves calculated with 30 and 50 levels of recursion for *d* electrons (the total energy minimum goes up). This is because in the latter case the continued fractions experience more reflections from the cluster boundaries that lead to an accumulation of errors. The increase of the size of the cluster from 1000 to 2000 atoms improves the accuracy (the total energy minimum goes down), but a further increase up to 10 000 atoms does not. For clusters of 1 000 atoms and more, the absence of periodic cluster boundary conditions does not noticeably change the calculated results. Therefore, in contrast to **k**-space band structure methods, for systems where periodic boundary conditions cannot be applied, free cluster boundary conditions can be used without a significant loss of accuracy. This advantage of the

method is especially useful for calculations of the electronic structure of dislocations, where lattice distortions are so long-ranged that even for very large clusters it is not possible to impose supercell boundary conditions in directions perpendicular to the dislocation axis, without artificially distorting the dislocation structure.

Based on these test calculations on bulk NiAl, balancing the computation time and accuracy, the optimal parameters can be chosen for calculations of the electronic structure of dislocations. Note, however, that since the differences in total energy at the equilibrium lattice constant calculated with a variety of parameters are very small, i.e., within 1 mRy, the TB-LMTO-REC method is, in fact, not very parameter sensitive.

For calculations of the electronic structure of dislocations, we applied an ''embedded cluster'' technique. A smaller cluster, including the atoms from the center of the dislocation with the most lattice distortions, is embedded in the larger cluster, representing the piece of bulk material with a single dislocation. We took advantage of the LMTO Hamiltonian, which can be divided into potential and structural parts, each calculated independently. The structural part is represented by screened structure constants, depending only on atomic coordinates and not on the type of atoms, and was calculated for all atoms in the larger cluster. Thus, very long-ranged structural distortions caused by dislocations were exactly taken into account in the structural part of the real-space TB-LMTO Hamiltonian. The potential part of the Hamiltonian is represented by potential parameters determined self-consistently from solution of the radial part of the Schrödinger equation for the embedded cluster, considering all atoms there as nonequivalent; for all other atoms in the larger cluster they were fixed equal to those in the bulk material. Within the embedded cluster, the atomic sphere radii were calculated according to the charge neutrality condition, and were fixed outside of the inner cluster. The size of the embedded cluster was chosen large enough to guarantee that perturbations of the potential due to the dislocation core are mostly confined within that cluster. The choice was made by comparing the potential parameters and atomic radii (which are an indirect indication of charge transfer) for atoms near the boundary of the embedded cluster and their nearest neighbors outside the embedded cluster. To be able to compare the total energies in different configurations, the embedded cluster was chosen to preserve the stoichiometry of the bulk material.

Depending on the complexity of the dislocation core structure, the size of the cluster was taken from about 10 000 to up to 22 000 atoms for dislocations with $\langle 100 \rangle$ and $\langle 111 \rangle$ Burgers vectors, respectively, and the embedded cluster (or self-consistency region) contained from about 120 nonequivalent atoms for $\langle 100 \rangle$, and up to 500 atoms for $\langle 111 \rangle$ dislocations. Periodic boundary conditions were imposed in the direction of the dislocation axis, and free boundary conditions in the two other directions. Calculations were carried out self-consistently until convergence, which was assumed when the total energy variation between subsequent iterations became less than 1 mRy. It usually took about 150 iterations to reach convergence.

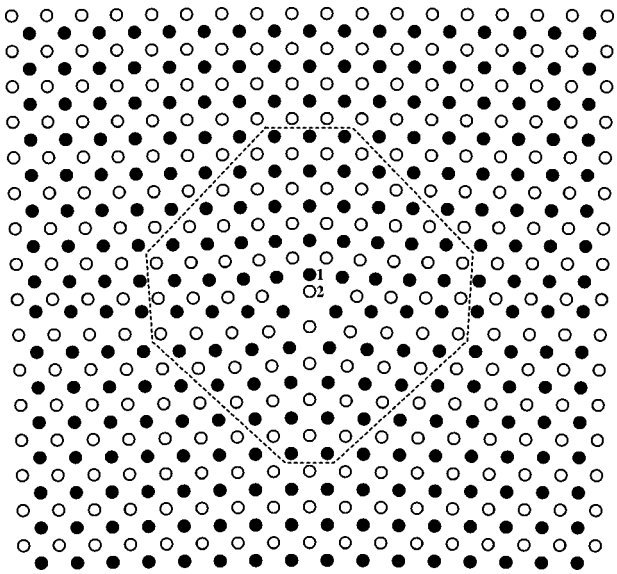

FIG. 2. Model of the $\langle 100 \rangle \{010\}$ edge dislocation in NiAl; the embedded cluster is outlined by dashed lines.

The atomic coordinates were determined within the Peierls-Nabarro (PN) model with dislocation structure parameters obtained from *ab initio* calculations of the generalized stacking fault (see Ref. 34 for more details). The structure of the dislocation determined within this approach corresponds to the minimum energy configuration resulting from a balance of elastic and atomic restoring forces.[18] Note that in general despite its simplicity, the PN model allows quite reasonable determinations of dislocation structure—especially with an accurate *ab initio* parametrization.[34,36–38] In the particular case of dislocations in NiAl, a comparison with atomistic simulations,[39] which are free from the PN model approximations but rely on interatomic interaction models, also suggests that the PN model does describe the structure of dislocations in a quite reasonable manner. In the PN model, lattice distortions caused by the dislocation are confined within the direction of the dislocation Burgers vector, and no atomic relaxations were taken into account. A limited atomic relaxation was later applied by optimizing the position of the central atom of the dislocation core in order to estimate the effect of relaxation on the electronic structure and the energy of the dislocation core, as described in the next section.

III. COMPUTATIONAL RESULTS

A. $\langle 100 \rangle \{010\}$ edge dislocation

The model of a $\langle 100 \rangle \{010\}$ edge dislocation in NiAl consisted of two nonequivalent (010) planes, perpendicular to the dislocation axis; each of them is monoatomic (i.e., filled either with Ni or Al atoms). In Fig. 2, the actual model used in calculations is shown, with the embedded cluster boundaries marked by dashed lines (note that, although both atomic planes are drawn together, they are shifted in the z direction by $\frac{1}{2}$ of the lattice parameter). The upper and lower layers are marked by black and open circles, respectively.

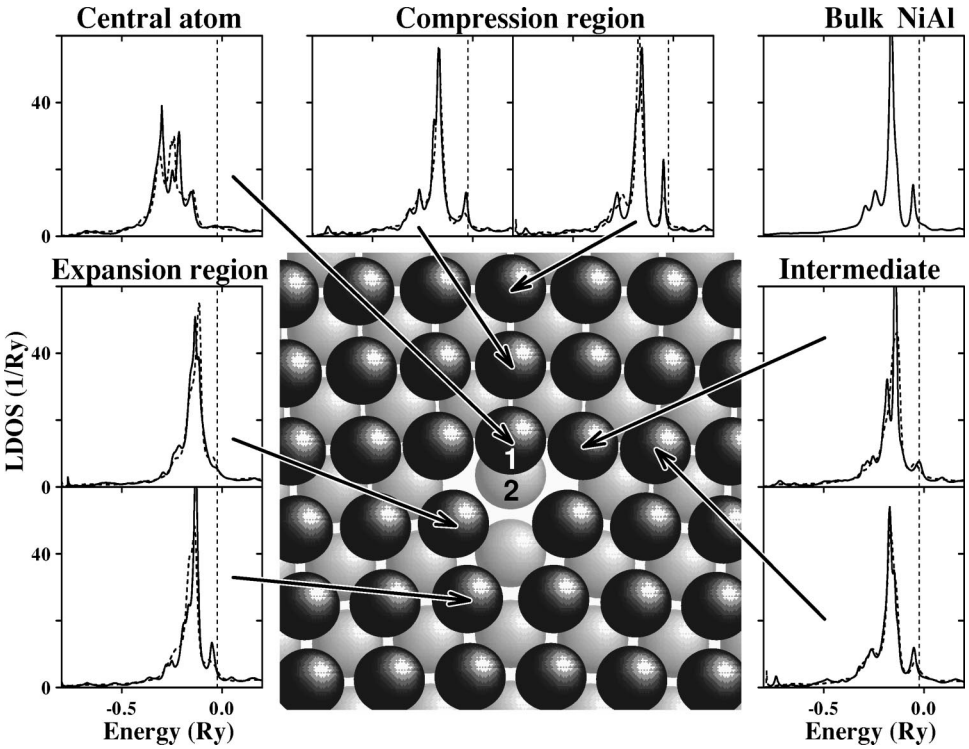

FIG. 3. LDOS for Ni atoms in the core of the ⟨100⟩{010} edge dislocation in NiAl, configuration A. Solid line: unrelaxed results, dashed line: after optimization of the position of atom 1.

Two nonequivalent dislocation core configurations are possible in NiAl: (i) the upper layer filled with Ni atoms (which we denote as configuration A) and (ii) the upper layer filled with Al atoms (which we denote as configuration B). The atom at the end of the extra plane is marked 1 and will also be referred to throughout the paper as the ''central atom of the dislocation core''; its nearest neighbor from the next plane is marked 2.

We first consider configuration A. In Figs. 3 and 4, the local densities of states (LDOS) for Ni and Al atoms in the dislocation core are presented along with the DOS for Ni or Al atoms in bulk NiAl, given for comparison. The most notable features of the calculated electronic structure is the formation of a well-defined peak (at -0.3 Ry) on the central Ni atom of the dislocation core, which is absent from the DOS of the parent crystal and all other Ni atoms beyond the

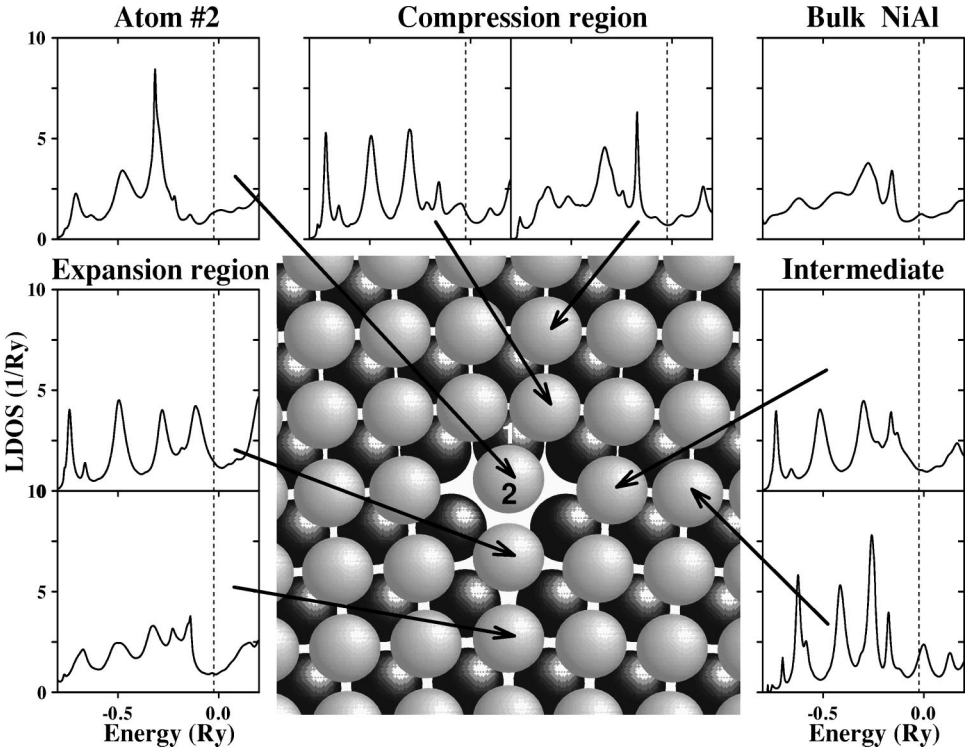

FIG. 4. LDOS for Al atoms in the core of the ⟨100⟩{010} edge dislocation in NiAl, configuration A.

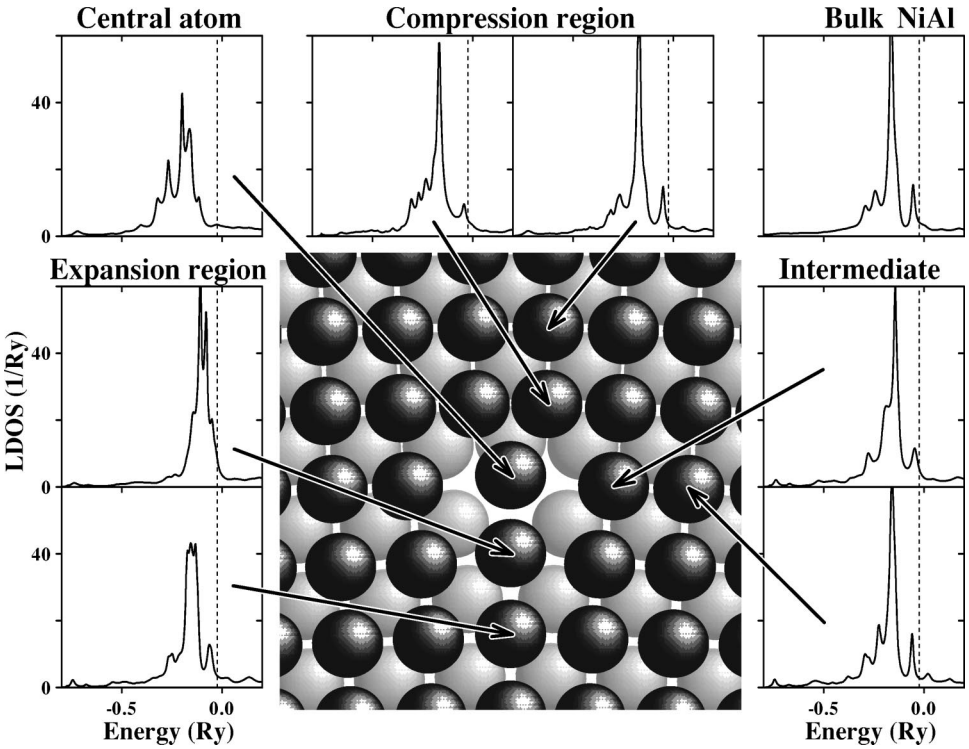

FIG. 5. LDOS for Ni atoms in the core of the $\langle 100\rangle\{010\}$ edge dislocation in NiAl, configuration B.

central atom. The electronic states corresponding to such a peak, resulting from local distortions of ideal spatial periodicity, were first described by Friedel as ''virtual bound states,''[40] and at present are called ''quasilocalized states'' (see, for example, Ref. 41). This term pertains to spatially local electronic states for which the DOS is characterized by a sharp and narrow peak (with energy E_{loc} and half-width Γ) embedded in a relatively broad band of itinerant electrons. According to the uncertainty relation, the electron resides in the state with energy E_{loc} for a time $\approx\hbar/\Gamma$. If Γ is sufficiently small (as in the present case), the lifetime of electron in the state with energy E_{loc} is relatively large, and therefore it is assumed that the electron is virtually localized. Hence, the term ''localized states'' is often used to describe quasilocalized electronic states resulting from the deviations from crystal symmetry due to point or extended defects, and so we will also use this terminology here for simplicity.

Previously, Eberhart and Vvedensky[3] observed the appearance of near-Fermi level localized states on grain boundaries in intermetallics. In contrast, the localized electronic states on $\langle 100\rangle\{010\}$ edge dislocations in NiAl appear deep inside the valence band, which is the result of peculiarities of the geometry of the dislocation core. Note that atom 1 has only six nearest neighbors compared to eight in bulk NiAl. Hence, this effect may be associated with the so-called ''broken bonds,'' or a change of coordination number in comparison with the bulk. In other words, the distortions in the center of the dislocation core lead to a situation with ''missing'' nearest neighbor atoms.[21] As stated in the Introduction, the localized states related to the ''broken bonds'' in the core of the edge dislocation are thought to be typical for semiconductors and covalent systems,[14] but this result is unusual for metallic systems, because of the common presumption that these effects will be screened by itinerant electrons.[19]

The Al LDOS (Fig. 4) for atom 2 is also characterized by the sharp peak at -0.3 Ry, that corresponds to the position of the localized peak in the Ni LDOS on atom 1, and the center of gravity of the occupied band is shifted to lower energy. Therefore, the severe transformation of electronic structure in the dislocation core is not limited to the central atom, but also includes its nearest neighbors. Overall, the perturbation of the LDOS on Al atoms caused by the dislocation is more long-ranged than for Ni atoms. However, the amplitude of the Al DOS is several times smaller than the Ni DOS; hence they give a much smaller contribution to the total dislocation DOS than do Ni atoms, and so we will mostly concentrate on the Ni DOS in our further descriptions.

Figure 5 shows the LDOS for Ni atoms for the $\langle 100\rangle\{010\}$ edge dislocation in configuration B. Here one can see again the peak of localized electronic states in the LDOS of the central atom of the dislocation core at an energy of -0.26 Ry; however, this peak is less pronounced than for configuration A. Another notable feature of the electronic structure of the dislocation core is connected with the LDOS of the atom in the expansion region, which is characterized by a significant narrowing of the *d* band and its shift to higher energy. This is a direct consequence of the increase of the distance between Ni and its nearest Al neighbors, resulting in a weakening of Ni-Al bonding and a decrease of hybridization. The same effect is also observed for configuration A (Fig. 3), but to a lesser degree because of a smaller expansion around the Ni atoms in this configuration.

Consider now other important dislocation-induced peculiarities of local electronic structure, namely, those connected with electronic states near the Fermi level (E_F). The electronic structure of bulk NiAl is characterized by a van-Hove singularity (vHS) below E_F, a feature known to be rather

typical for metallic systems (see Ref. 42). Lattice distortions in the dislocation core lead to the existence of both compression and expansion regions near the core. There is a possibility that these dilatations may result in a shift of the vHS onto E_F for some atoms near the core. Our *ab initio* calculations support such a scenario for some Ni atoms in the dislocation core with configuration A (see the LDOS for atoms in a region of ''compression'' and in the intermediate region). These features may result in important contributions to the scattering of electrons by dislocation cores and thus, may possibly be revealed in measured transport properties of real metallic materials.

On the other hand, the appearance of LDOS peaks at E_F is usually considered as evidence of the instability of a given structure,[42] and so one may expect that structural relaxation of the dislocation core may lead to a stabilization of the configuration. Obviously, the atomic structure used and the electronic structure were obtained in different frameworks. The determination of both the atomic and electronic structures in the same computation scheme should lead to a configuration with lower energy than that generated within the PN model. Unfortunately, there are no easy ways to perform structural optimization in the framework of the TB-LMTO-REC method because of deficiencies of the atomic sphere approximation, which cannot give accurate atomic forces. Another way to find the optimized structure—by moving atoms and finding their optimal positions with respect to the total energy minimization—will require many-parameter optimizations and a tremendous number of self-consistent calculations, which is hardly possible to implement.

Hence in this work, we restricted ourselves to optimizing the position of the central atom in the dislocation core (atom 1) only. Because it is the atom on which localized states were found, we assume that optimization of its position will have the largest impact on the electronic structure and energetics of the dislocation core. Taking into account the presence of a symmetry in the dislocation core, the optimized position of this atom was searched by moving it along the [001] axis in both directions. For each position of the atom, full self-consistent calculations of the resulting atomic configuration were made, and total energies were calculated. It is known that the ASA may lead to errors in total energy determinations, especially in systems with large distortions away from close packing (which is a feature of the dislocation core).

To verify the reliability of our total energy calculations, we have also performed a set of calculations employing the local force theorem[43] (LFT) for the same configurations. We made one iteration of the self-consistent calculations starting from the bulk NiAl potential, keeping the atomic sphere radii equal to those of NiAl, so that the only variational parameter was the change of structure. The computational results are presented in Fig. 6, where the difference between the total energy of the embedded cluster with a dislocation and the cluster of the same size in ideal NiAl is plotted as a function of the displacement of atom 1. One can see that both the total energy and LFT energy-displacement curves have the same character and give the same optimized position of atom 1. There are very large changes in the dislocation core energy due to displacement of the central atom in the dislocation core. This is the result of very large and specific changes in the local electronic structure of this atom, which contribute significantly to the total energy changes. After optimization, however, the total energy of the dislocation core with the optimized position of atom 1 is only slightly higher than those for bulk NiAl itself—which indicates that the effect of the relaxation of all the other atoms will be small.

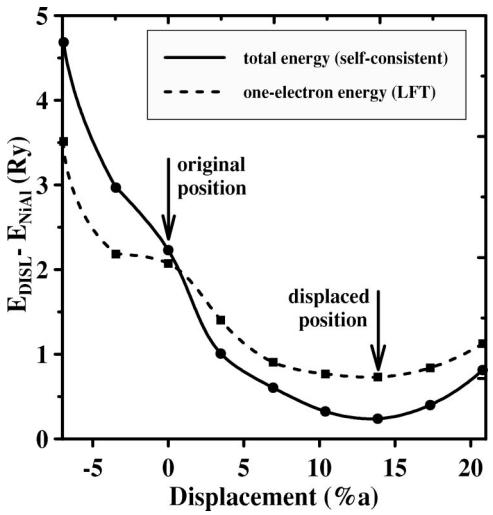

FIG. 6. Changes of the energy of the ⟨100⟩{010} edge dislocation in NiAl due to displacement of the central atom of the core.

The large displacement of the central atom due to relaxation from its original position given by the PN model (0.04 nm, or about 14% of the lattice parameter) may reflect an inaccuracy of the dislocation core description within the PN model. It is, however, certainly a definite indication of the large electronic contribution to the dislocation energy. Nevertheless, despite the large quantitative changes in the energy of the dislocation core due to relaxation, the picture of the electronic states remains quantitatively the same. Since we concentrate in the present paper on the peculiarities of the electronic structure of the dislocation core rather than on its energetics, the use of the PN model of dislocations in our calculations seems appropriate.

This conclusion is also confirmed by a study of the LDOS in the dislocation core for the configuration with the optimized position of the central atom shown in Fig. 3. One can easily notice that the localized states peak is still present on the central atom; only their amplitude is somewhat decreased and their positions are slightly changed. This result strongly supports our suggestion that the nature of states is not the result of a nonequilibrium configuration of the dislocation core. As for atoms for which a shift of vHS peaks to E_F was observed, the relaxation causes these states to move slightly below E_F, decreasing the number of states at E_F and increasing the stability of the configuration.

B. ⟨111⟩{011} edge dislocation

To clarify the dependence of the local electronic structure on the kind of dislocation and especially on the atomic coordination in the core, we have also performed calculations

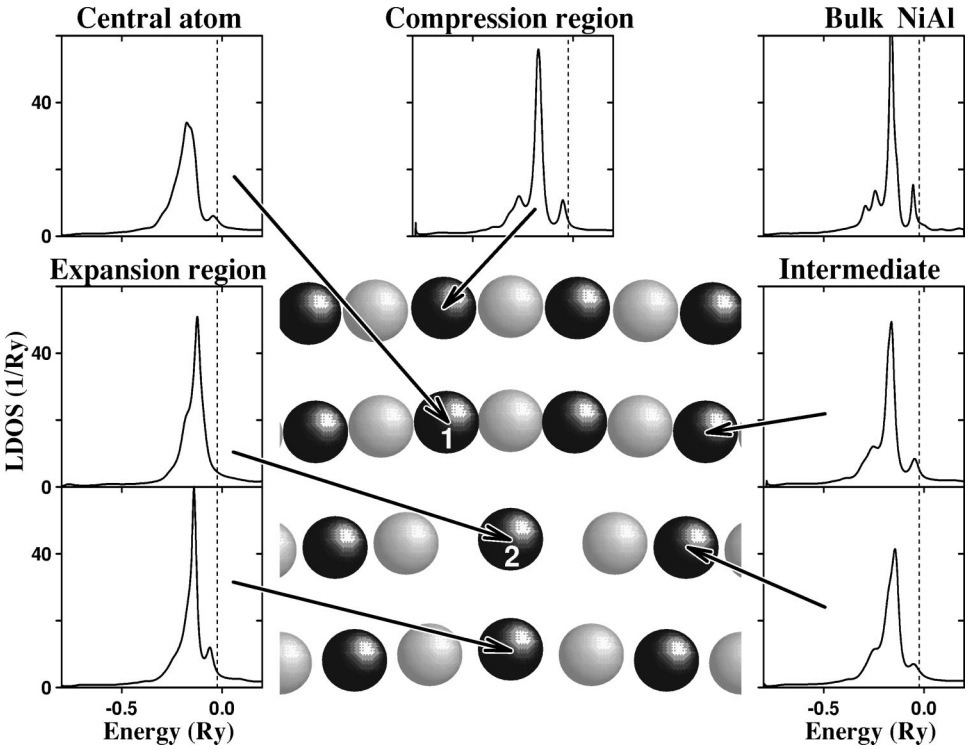

FIG. 7. LDOS for Ni atoms in the core of the ⟨111⟩{110} edge dislocation in NiAl.

of the electronic structure of the ⟨111⟩{011} edge dislocation in NiAl. The structural model for this dislocation consists of six nonequivalent (112) planes. The ⟨111⟩{011} edge dislocation is split into two superpartials with a distance between them of the order of the width of the core (which, in this case, is equal to the lattice parameter). The splitting of the ⟨111⟩{011} dislocation produces an antiphase boundary (APB) in the core, which has a significant impact on the properties of this dislocation and defines the splitting width.

The LDOS for the Ni atoms in one atomic plane in the region of the dislocation core is presented in Fig. 7. The most striking result is that there are no localized states for those atoms in the core which have ''broken bonds.'' Instead, the LDOS has a single structureless peak (the antibonding peak and a pseudogap between bonding and antibonding peaks also almost disappear). This is in drastic contrast with the results for the ⟨100⟩{010} edge dislocation, where well-defined localized states were observed—which leads to the conclusion that the presence of ''broken bonds'' in the dislocation core itself cannot guarantee the appearance of localized states in metals. Several factors resulting from differences in the Burgers vector direction and glide plane orientation between the ⟨111⟩{110} and the ⟨100⟩{010} edge dislocations, may lead to differences in the LDOS, namely, (i) the longer periodicity in the dislocation axis direction (6 layers vs 2), (ii) the interplay between superpartial dislocations, (iii) different local nearest-neighbor configurations, and (iv) the presence of an APB.

The last two factors seem to be the most important, since it is well-known that the major features of the local electronic structure of an atom in a solid are determined by its interactions with nearest neighbors. The presence of an APB in the dislocation core changes the occupancy of some second nearest neighbors by replacement of one Ni atom with an Al atom; hence the resulting bond between this Al atom and the central Ni atom can bind extra electrons due to broken Ni-Al bonds in the first neighbor shell, and so prevent them from localization. The similarity between the LDOS on the central atom 1 in the core and atom 2 from the expansion region, both of which are closest to the APB, supports this point of view.

The role of other factors on the electronic structure is not clear because the differences in the Burgers vector and slip plane directions in these dislocations makes their direct comparison rather complicated. To clarify the role of these geometrical factors, we have performed electronic structure calculations for the ⟨100⟩{011} edge dislocation, which may be considered (in some sense) as an ''intermediate'' case between the two edge dislocations studied above.

C. ⟨100⟩{011} edge dislocation

The ⟨100⟩{011} edge dislocation, along with the ⟨100⟩{010} edge dislocation, is the most often observed slip system in NiAl crystals. The model employed consists of two nonequivalent $(01\bar{1})$ planes. The LDOS for Ni atoms in the central part of the dislocation core are presented in Fig. 8; its most interesting peculiarities are that again we see the appearance of localized states on the central atom in the dislocation core, though they are less pronounced than for the central atom of the ⟨100⟩{010} edge dislocation. This atom can also be described as having ''broken bonds.'' The LDOS on other atoms in the core (both Ni and Al) are also less perturbed than in the ⟨100⟩{010} edge dislocation, and there are no significant changes in the electronic states near the Fermi energy.

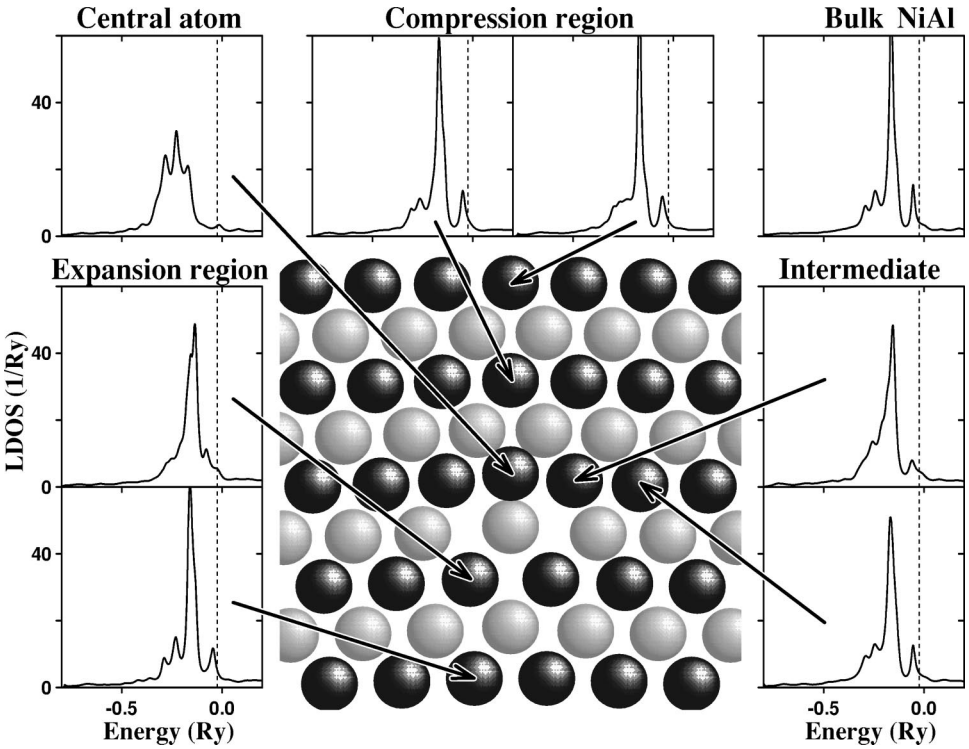

FIG. 8. LDOS for Ni atoms in the core of the ⟨100⟩{011} edge dislocation in NiAl.

IV. MECHANISM OF ELECTRON LOCALIZATION ON DISLOCATIONS AND COMPARISON WITH BCC TRANSITION METALS

In comparing the computational results for the different types of dislocations investigated one can see that while ''broken bonds'' are important, they are not the only factor determining the appearance of localized electronic states in the dislocation core. In particular, whereas there are atoms with ''broken bonds'' for all the edge dislocations considered, the localization takes place only for ⟨100⟩{010} and (to a lesser degree) ⟨100⟩{011}. A comparison of atomic core configurations for different types of dislocations allows us to conclude that the second factor controlling the appearance of localized electronic states is the local symmetry of atoms in the core. Our computational results show that the localized states only appear provided that the first neighbor shell in the dislocation core possesses mirror symmetry with respect to the reflections in the extra plane.

To understand how the observed features of the electronic structure of dislocation cores are connected with the local atomic structure, we considered the nearest neighbor configurations of central atoms in the dislocation cores for different types of dislocations [Figs. 9(b)–9(d)]. In Fig. 9(a) the nearest neighbors of Ni in ideal NiAl are shown for comparison. If we put the nickel atom in the center of a cube representing the NiAl unit cell, its first eight nearest Al neighbors will occupy eight cube edges. In the core of the ⟨100⟩{010} edge dislocation in configuration A [Fig. 9(b)], the nearest neighbor configuration changes significantly: the four Al atoms on the upper face of the cube remain almost unchanged, but two Al atoms from the lower face are absent (''broken bonds'') and two remaining Al atoms are shifted from their original positions at the cube corners to the positions close to the centers of the cube edges, as marked by arrows. The mirror symmetry with respect to the extra plane is present here, and localized electronic states are observed for this dislocation.

In the ⟨111⟩{011} case, for which electron localization is not observed, two Al atoms from the lower cube face are also absent [Fig. 9(c)], however, the remaining two Al atoms keep their original positions at the cube edges. Finally, for the ⟨100⟩{011} dislocation, the local atomic structure is in-

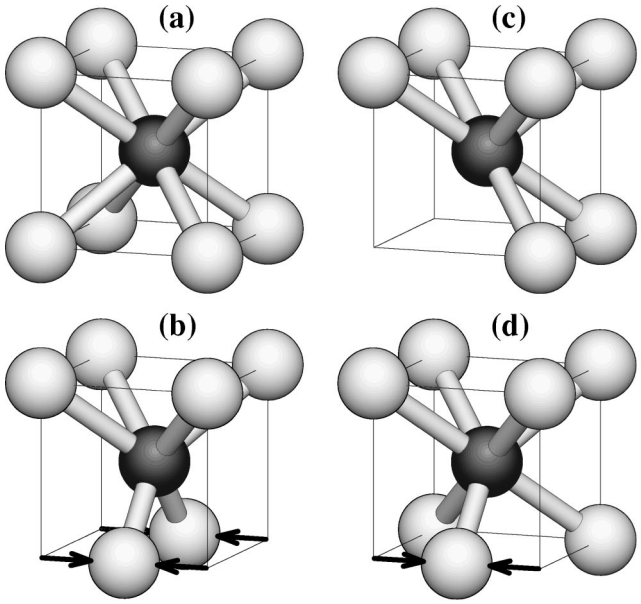

FIG. 9. Local nearest neighbor configurations for Ni atoms in (a) bulk NiAl; central Ni atoms of the core of (b) the ⟨100⟩{010}, (c) ⟨111⟩{011}, and (d) ⟨100⟩{011} edge dislocations in NiAl.

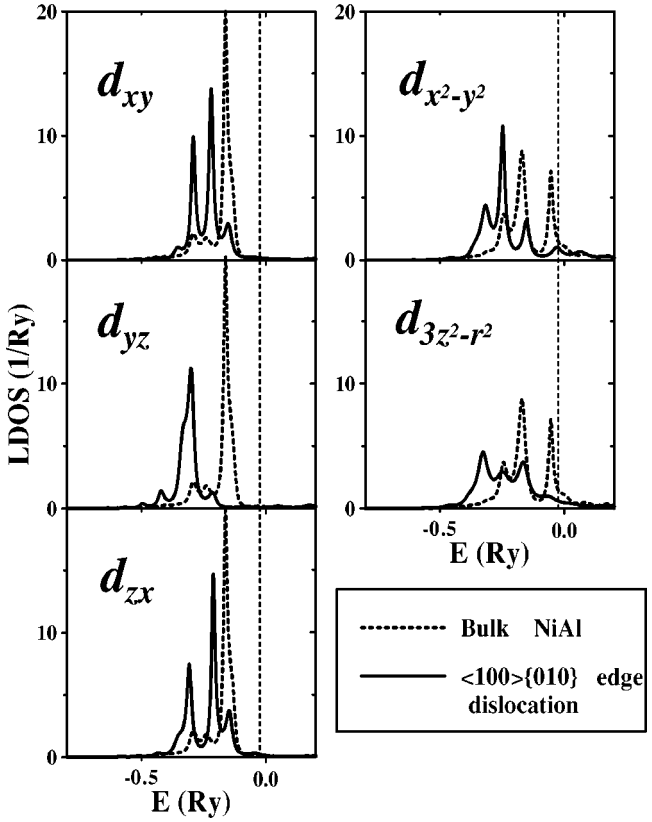

FIG. 10. Partial LDOS for *d* states on the central Ni atom in the $\langle 100\rangle\{010\}$ edge dislocation core in NiAl compared with Ni *d*-PDOS in bulk NiAl.

termediate between ideal NiAl and the $\langle 100\rangle\{010\}$ dislocation. Only one ''broken bond'' is present here, and one Al atom is moved to the position at the center of the cube edge. The mirror symmetry with respect to the extra plane remains.

The observed correlation between the local atomic symmetry of the nearest neighbor configurations of central atoms and the local electronic structure led us to the assumption that the orientation of interatomic bonds with respect to the geometry of the electronic *d* orbitals of the central atom of the dislocation core plays the important role in the appearance of the localized electronic states.

In Fig. 10, the orbital-projected *d* electron partial densities of states (PDOS) for the central atom of the dislocation core are shown in comparison with those for Ni in bulk NiAl. One can see that since the original B2 crystal symmetry is broken, the *d*-state degeneracy is removed for both the e_g (right panel) and t_{2g} (left panel) states. The most dramatic changes are observed for the t_{2g}-type orbitals, where the d_{xy} and d_{zx} orbitals form two distinct peaks, and the d_{yz} orbitals form a single peak that gives the largest contribution to the localized electronic states. By comparing the spatial geometry of the d_{yz} orbital and the local atomic geometry around the central atom of the dislocation core (Fig. 11), one can see that the d_{yz} orbital becomes oriented along the Ni-Al bond for the $\langle 100\rangle$ dislocations [see Figs. 9(b),9(d)]. As a result, a direct overlap between Ni d_{yz} and Al *s* is formed. The overlap between the Ni d_{yz} and Al p_y and p_z orbitals also increases. Extra electrons from the broken bonds form preferred bonding along the Ni-Al bond, leading to spatial and energetic electron localization. It should be especially stressed that the spatial electron localization takes place not on the Ni atom alone, but along the Ni-Al bond and the peak of localized electronic states appears on the Al atom 2 in Fig. 4. The changes in the e_g states are mainly in their shift to lower energy.

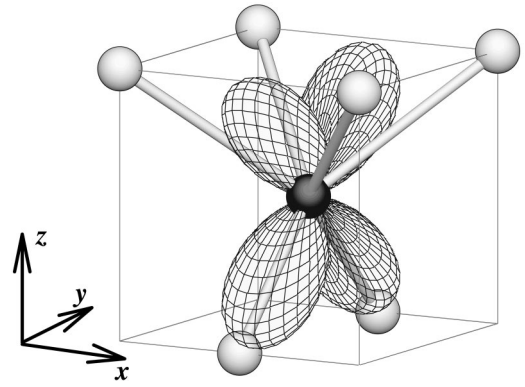

FIG. 11. d_{yz} orbital configuration of the central Ni atom in the $\langle 100\rangle\{010\}$ edge dislocation core in NiAl.

In the case of the $\langle 111\rangle\{011\}$ edge dislocations, there are no geometric rearrangements leading to the formation of preferred bonding, and extra electrons from ''broken bonds'' are being screened, or redistributed along the other atoms, in accordance with conventional metal theories. Thus, our results for the $\langle 100\rangle$ edge dislocation are not in contradiction with these theories, but rather demonstrate that a new phenomenon is taking place due to specific lattice distortions and atomic rearrangements in the core of the $\langle 100\rangle$ edge dislocations.

Based on the mechanism responsible for the localization in NiAl proposed above, one can suppose that the replacement of the Al atom, that belongs to the bond with electron localization, by another Ni (or other *d* element) atom may lead to even stronger electron localization due to the formation of direct overlap between two d_{yz} orbitals of two Ni atoms. This situation may take place, for example, in nonstoichiometric Ni-rich NiAl alloys. To test this possibility, we performed electronic structure calculations for the $\langle 100\rangle\{010\}$ edge dislocation in hypothetical bcc Ni. This was modeled by the replacement of all Al atoms by Ni atoms in NiAl with $\langle 100\rangle\{010\}$ edge dislocation and the adjustment of the lattice parameter for the theoretically calculated equilibrium lattice parameter for bcc Ni.

The LDOS for the central atom of the dislocation core is shown in Fig. 12 in comparison with the calculated DOS for bulk bcc Ni. Pronounced localized electronic states peaks can be seen near the bottom of the *d* band for the central atom of the core. The *d*-orbital PDOS for the central atom of the dislocation core is also shown in Fig. 12. As expected, the most pronounced localization is observed for the d_{yz} orbitals, where sharp peaks are present near the very bottom of the *d* band. There is also a visible increase of the band width accompanied by an increase of the splitting between bonding and antibonding states, which is an indication of the increase of hybridization between d_{yz} states of this atom and its neighbor. These results support our conclusion about the

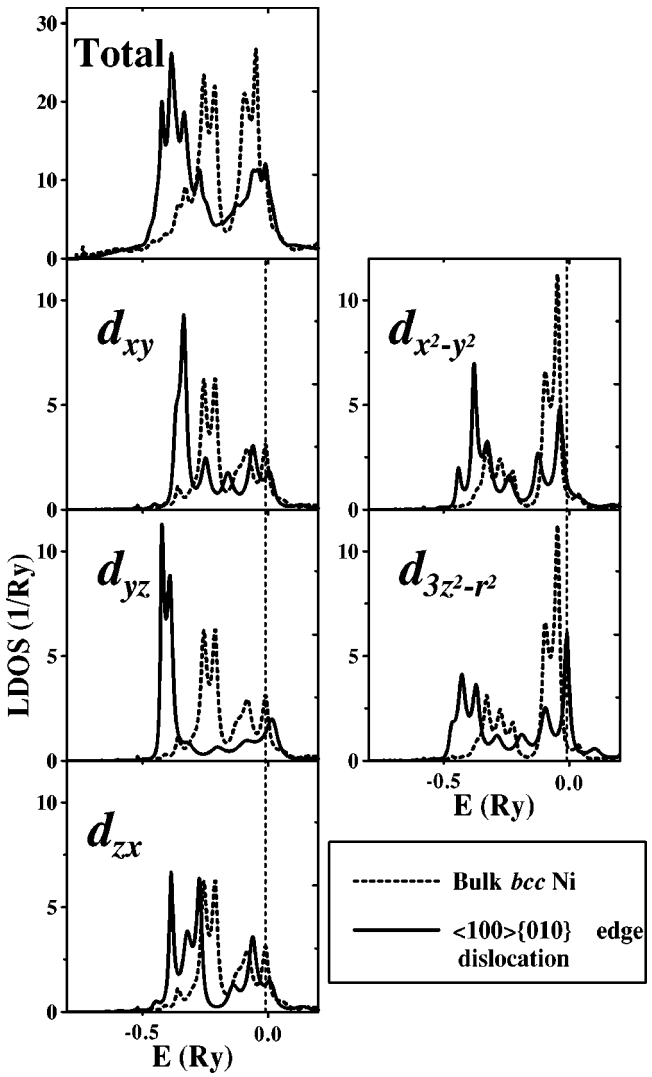

FIG. 12. Total and partial *d* states LDOS on the central atom in the ⟨100⟩{010} edge dislocation core in bcc Ni compared with bulk bcc Ni.

causes of electron localization on ⟨100⟩ dislocations. Geometric configurations necessary for electron localization, will be realized by edge dislocations with ⟨100⟩ Burgers vector in materials with bcc or $B2$ structure. The presence of the *d* element is another factor leading to strong localization.

To verify our conclusions on real bcc metals, we performed electronic structure calculations for the ⟨100⟩{010} edge dislocations in bcc Fe and W. Even more pronounced than for Ni, very strong electron localization is observed for Fe. For the 5*d* element W, which has fewer electrons in the valence band than Fe and Ni, the peaks of localized electron states are less pronounced, but are still very distinctive.

V. DISCUSSION AND CONCLUSION

The results obtained demonstrate that the introduction of dislocations in metals leads to a significant local reconstruction of the electronic states. For dislocations with ⟨100⟩ Burgers vector in transition metals and alloys with bcc-type lattice, this reconstruction is accompanied by an unusual peculiarity, namely, the formation of localized electronic states inside the valence band. The conditions for the appearance of these states are (i) a decrease of the number of nearest neighbors (the number of bonds) around the central atom of the dislocation core, (ii) a specific local symmetry of the atomic arrangement in the region of the dislocation core, and (iii) the contribution of *d* states to the formation of these interatomic bonds. Elastic lattice distortions around an edge dislocation also influence the electronic spectrum (especially near E_F), but are not responsible for electron localization.

The conditions for the appearance of localized electronic states are satisfied for ⟨100⟩ edge dislocations with {010} and {011} slip planes which have a local atomic configuration with some of the bonds aligned along one of the t_{2g} orbitals. For dislocations with Burgers vector parallel to ⟨100⟩, the local symmetry of the atomic arrangement is different, and so one of the conditions outlined above is not satisfied. Namely, the mirror symmetry with respect to the extra plane is not present, the bonds do not align parallel to t_{2g} orbitals, and localized electronic states do not appear.

The most important difference between electron localization on dislocations in semiconductors and metals is that in semiconductors localized electronic states arise due to nonbonding orbitals resulting from broken covalent bonds.[44] Unpaired electrons localize on these bonds, and since they do not participate in chemical bonding, their electronic spectrum usually has the form of a single δ-function-like peak in the band gap. In metals, as demonstrated above, spatial electron localization takes place on bonding orbitals between the central atom of the dislocation core and its first nearest neighbor. Therefore, localized electrons will participate in chemical bonding and may potentially have impact on how physical properties of metal change upon alloying. In metals, localized electronic states will also have a much more influence on dislocation energetics, than in semiconductors. Since these states appear inside the valence band, they will have a significant influence on the dislocation energy—both directly, changing the band energy, and indirectly, through the hybridization and charge transfer.

Since *d* electrons give the main contribution to localized electronic states, one can expect that in $B2$ intermetallic alloys where both elements are transition metals this effect will be more pronounced than in NiAl. Therefore the effects connected with electron localization can be more naturally expected in other $B2$ intermetallics, such as CoTi, CoHf, and CoZr,[23] where the deformation is also carried by ⟨100⟩ edge dislocations. The presence of two sorts of atoms is not necessary; localized electronic states appear also in monoatomic bcc transition metals. However, ⟨100⟩ dislocations are not typical for bcc metals; they do not participate in plastic deformation. They can appear, however, as elements of dislocation walls after special preparation, which includes high-temperature annealing.[45]

Let us briefly discuss the effect of electronic structure changes near the dislocation on macroscopic properties. Changes of the LDOS near E_F should, in principle, reveal themselves in many physical properties of metals, especially transport (electroconductivity, thermopower, etc.), magnetic,

and so on. According to common views, the dislocation core, rather than the long-ranged deformation field, gives the main contribution to the electroresistivity.[46] At present, however, there is no adequate model of electron scattering on the dislocation core. The results presented here open possibilities for more consistent considerations of this problem.

The peak of the LDOS corresponding to localized electronic states is located inside the valence band and cannot directly influence the transport properties. However, the presence of localized electronic states may contribute significantly to the dislocation energetics and impurity-dislocation interactions.[21] Our results support this point of view. Indeed, suppose that during the glide a ⟨100⟩ edge dislocation encounters a transition metal impurity *X* substituting the atom in the Al sublattice. As a result, the Ni-Al bond in the dislocation core will be substituted by a Ni-*X* bond. This will lead to an increase of the electron localization and a decrease of the one-electron contribution to the total energy. Recently,[47] we have demonstrated for early transition metal impurities (Ti, V) that the strong hybridization (resonance) between impurity electronic states and dislocation localized states leads to a dominant contribution to the impurity-dislocation interaction energy. These findings showed that electron localization on ⟨100⟩ edge dislocations is responsible for the mechanisms controlling the ''extra'' solid-solution hardening phenomena[6,7] and the observed[48] anomalous increase of creep resistance upon alloying in NiAl and intermetallic alloys.

ACKNOWLEDGMENTS

This work was supported by the Air Force Office of Scientific Research under Grant No. F49620-98-1-0321, by the National Science Foundation under Cooperative Agreement No. ACI-9619019, through the University of Illinois, and in part by the Russian Basic Research Foundation under Grant No. 01-02-16108; it utilized the Origin2000 at the NSF supported National Center for Supercomputing Applications, University of Illinois at Urbana-Champaign, and at the Naval Oceanographic Office (NAVO).

[1] G.L. Krasko and G.B. Olson, Solid State Commun. **76**, 247 (1990).
[2] R. Wu, A.J. Freeman, and G.B. Olson, Science **265**, 376 (1994).
[3] M.E. Eberhart and D.D. Vvedensky, Phys. Rev. Lett. **58**, 61 (1987).
[4] T. Shinoda, K. Masuda-Jindo, Y. Mishima, and T. Suzuki, Phys. Rev. B **35**, 2155 (1987); T. Shinoda, K. Masuda-Jindo, and T. Suzuki, Philos. Mag. B **62**, 289 (1990).
[5] O.Yu. Kontsevoi, O.N. Mryasov, Yu.N. Gornostyrev, A.J. Freeman, M.I. Katsnelson, and A.V. Trefilov, Philos. Mag. Lett. **78**, 427 (1998).
[6] Y. Mishima, S. Ochai, N. Hamano, Y. Yodogava, and T. Suzuki, Trans. Jpn. Inst. Met. **27**, 648 (1986).
[7] V.O. Abramov and O.V. Abramov, Dokl. Akad. Nauk SSSR **318**, 883 (1991) [Sov. Phys. Dokl. **36**, 454 (1991)].
[8] M.I. Kaganov, V.Ya. Kravchenko, and V.D. Natsik, Usp. Fiz. Nauk **111**, 655 (1973).
[9] S.G. Roberts, P. Pirouz, and P.B. Hirsch, J. Mater. Sci. **20**, 1739 (1985).
[10] V.I. Altshits, E.V. Darinskaya, and O.L. Kazakova, Zh. Eksp. Teor. Fiz. **111**, 615 (1997) [JETP **84**, 338 (1997)]; Yu. I. Golovin, R. B. Mogutnov, A.A. Baskakov, and M.V. Badylevich, Pis'ma Zh. Eksp. Teor. Fiz. **69**, 114 (1999) [JETP Lett. **69**, 127 (1999)]; M. Molotskii and V. Fleurov, Phys. Rev. Lett. **78**, 2779 (1997).
[11] M.S. Duesbery, in *Dislocations in Solids*, edited by F.R.N. Nabarro (North-Holland, Amsterdam, 1989), Vol.8, p. 67.
[12] V. Vitek, Prog. Mater. Sci. **36**, 1 (1992).
[13] S. Ismail-Beigi and T.A. Arias, Phys. Rev. Lett. **84**, 1499 (2000).
[14] R. Labush and W. Shröter, in *Dislocations in Solids*, edited by F.R.N. Nabarro (North-Holland, Amsterdam, 1980), Vol. 5, p. 127.
[15] W. Shockley, Phys. Rev. **91**, 228 (1953).
[16] P.B. Hirsch, Mater. Sci. Technol. **1**, 666 (1985).
[17] N. Lehto and S. Öberg, Phys. Rev. B **56**, 12 706 (1997).
[18] J.P. Hirth and J. Lothe, *Theory of Dislocations* (Wiley, New York, 1982).
[19] J. Friedel, *Dislocations* (Pergamon Press, New York, 1964).
[20] N.I. Medvedeva, Yu.N. Gornostyrev, D.L. Novikov, O.N. Mryasov, and A.J. Freeman, Acta Mater. **46**, 3433 (1998).
[21] A.O. Anokhin, M.L. Galperin, Yu.N. Gornostyrev, M.I. Katsnelson, and A.V. Trefilov, Pis'ma Zh. Eksp. Teor. Fiz. **59**, 345 (1999) [JETP Lett. **59**, 198 (1994)]; Phys. Met. Metallogr. **79**, 242 (1995); Philos. Mag. B **73**, 845 (1996).
[22] Some of the results for ⟨100⟩{010} edge dislocation in NiAl have already been presented, in part, in Ref. 5.
[23] R.D. Noebe, R.R. Bowman, and M.V. Nathal, Int. Mater. Rev. **38**, 193 (1993).
[24] O.Yu. Kontsevoi, O.N. Mryasov, A.I. Liechtenstein, and V.A. Gubanov, Fiz. Tverd. Tela. (Leningrad) **34**, 293 (1992) [Sov. Phys. Solid State **34**, 154 (1992)].
[25] O.Yu. Kontsevoi, O.N. Mryasov, and V.A. Gubanov, Fiz. Tverd. Tela (Leningrad) **34**, 2624 (1992) [Sov. Phys. Solid State **34**, 1406 (1992)].
[26] H.J. Nowak, O.K. Andersen, T. Fujiwara, O. Jepsen, and P. Vargas, Phys. Rev. B **44**, 3577 (1991).
[27] O.K. Andersen and O. Jepsen, Phys. Rev. Lett. **53**, 2571 (1984).
[28] O.K. Andersen, O. Jepsen, and D. Glötzel, in *Highlights of Condensed Matter Theory*, edited by F. Bassani, F. Fumi, and M.P. Tosi (North Holland, New York, 1985), p. 59.
[29] R. Haydock, in *Solid State Physics*, edited by H. Ehrenreich, F. Seitz, and D. Turnbul (Academic, New York, 1980), Vol. 35, p. 216.
[30] U. von Barth and L. Hedin, J. Phys. C **5**, 1629 (1972).
[31] N. Beer and D.G. Pettifor, in *Electronic Structure of Complex Systems*, edited by P. Phariseau and W.M. Temmerman (Plenum, New York, 1984), p. 769.
[32] V. Sundararajan, B.R. Sahu, D.J. Kanhere, P.V. Panat, and G.P. Das, J. Phys.: Condens. Matter **7**, 6019 (1995).

[33] A.R. Williams, J. Kübler, and C.D. Gelatt, Phys. Rev. B **19**, 6094 (1979).
[34] N.I. Medvedeva, O.N. Mryasov, Yu.N. Gornostyrev, D.L. Novikov, and A.J. Freeman, Phys. Rev. B **54**, 13 506 (1996).
[35] R. Wu, L. Zhong, L.-J. Chen, and A.J. Freeman, Phys. Rev. B **54**, 7084 (1996).
[36] Y.-M. Juan and E. Kaxiras, Philos. Mag. A **74**, 1367 (1996).
[37] B. Joos, Q. Ren, and M.S. Duesbery, Phys. Rev. B **50**, 5890 (1994).
[38] O.N. Mryasov, Yu.N. Gornostyrev, and A.J. Freeman, Phys. Rev. B **58**, 11 927 (1998).
[39] M.J. Mills, M.S. Daw, S.M. Foiles, and D.B. Miracle, in *High Temperature Ordered Intermetallic Alloys V*, edited by I. Baker, R. Darolia, J.D. Whittenberger, and M.H. Yoo, MRS Symposia Proceedings No. 288 (Materials Research Society, Pittsburgh, 1993), p. 257.
[40] J. Friedel, Nuovo Cimento, Suppl. **7**, 287 (1958); A. Blandin and J. Friedel, J. Phys. Radium **20**, 160 (1959).
[41] S.V. Vonsovsky and M.I. Katsnelson, *Quantum Solid State Physics* (Springer, Berlin, 1989).
[42] S.V. Vonsovskii, M.I. Katsnelson, and A.V. Trefilov, Phys. Met. Metallogr. **76**, 247 (1993); M.I. Katsnelson, I.I. Naumov, and A.V. Trefilov, Phase Transitions **49**, 143 (1994).
[43] A.R. Mackintosh and O.K. Andersen, in *Electrons at the Fermi Surface*, edited by M. Springford (Cambridge University Press, Cambridge, 1980).
[44] H. Veth and H. Teichler, Philos. Mag. **49**, 371 (1984).
[45] I.M. Aristova and L.N. Pronina, Phys. Solid State **35**, 1340 (1993).
[46] R.A. Brown, Can. J. Phys. **60**, 766 (1982).
[47] O.Yu. Kontsevoi, Yu.N. Gornostyrev, A.J. Freeman, M.I. Katsnelson, and A.V. Trefilov, Philos. Mag. Lett. **81**, 455 (2001).
[48] P.H. Kitabjian, A. Garg, R.D. Noebe, and W.D. Nix, in *High Temperature Ordered Intermetallic Alloys VII*, edited by C.C. Koch, C.T. Liu, N.S. Stoloff, and A. Wanner, MRS Symposia Proceedings No. 460 (Materials Research Society, Warrendale, 1997), p. 479; Metall. Mater. Trans. A **30**, 587 (1999).